energy&fuels

Article

Cite This: Energy Fuels 2018, 32, 1155−1165

pubs.acs.org/EF

Understanding Model Crude Oil Component Interactions on Kaolinite Silicate and Aluminol Surfaces: Toward Improved Understanding of Shale Oil Recovery

Shansi Tian,[†,‡,§] Valentina Erastova,[∥] Shuangfang Lu,[*,†,‡] H. Chris Greenwell,[*,§] Thomas R. Underwood,[§] Haitao Xue,[†,‡] Fang Zeng,[‡] Guohui Chen,[†,‡] Chunzheng Wu,[†,‡] and Rixin Zhao[†,‡]

[†]Research Institute of Unconventional Petroleum and Renewable Energy (RIUP&RE), China University of Petroleum, East China, Qingdao 266580, Shandong PR China

[‡]School of Geosciences, China University of Petroleum, East China, Qingdao 266580, Shandong, PR China

[§]Department of Earth Science and [∥]Department of Chemistry, Durham University, Durham DH1 3LE, United Kingdom

Supporting Information

ABSTRACT: Shale oil is currently of interest for unconventional resource exploration and development. Understanding the mechanism of interaction between the complex mixture of organic compounds in shale oil and minerals making up the reservoir rock−oil interface will assist recovery. In this study, molecular dynamics simulation is used to study the adsorption characteristics of a model oil mixture within nanoscale intraparticle pores of kaolinite minerals, which form pore-filling structures in shale rock. To better understand the effects of oil composition, temperature, and pressure on the adsorption properties of the model oil mixture, a range of temperatures (298, 323, 348, and 373 K) and pressures (1, 50, 100, and 200 bar) representing up to reservoir conditions were used. This study shows that adsorption and arrangement of oil molecules is dependent on the surface of kaolinite and the distance away from it. The simulations show polar compounds are likely to be adsorbed on aluminol kaolinite basal surfaces, while alkanes preferentially adsorb on silicate surfaces. In addition, the number of oil-molecule-bound layers and the total adsorption amount on the silicate surface is greater than the aluminol surface. The density of adsorbed oil is reduced with increase in temperature, while the effect of pressure is not as significant. On the basis of performed molecular simulations, we show the adsorption rate of shale oil on the surfaces of kaolinite sheets and assess the capacity to remove the model oil.

1. INTRODUCTION

With increasing demand for energy, and while conventional oil and gas resources are being depleted, unconventional oil and gas are receiving more attention because they have become a major contributor to sustained growth in global hydrocarbon production. The exploration and development of shale gas has achieved notable success in North America[1−3] and led a global shale gas research boom.[4,5] However, with the lessons learned from initial phases of shale gas extraction and the decrease of natural gas price, investors have now shifted their attention to more profitable shale oil.[6−8] According to the Energy Information Administration,[9] in the last 10 years, the production of U.S. shale oil has increased 12.2 times to an average of 4.57 million barrels per day (MMbbl/day) in 2015, compared to 0.37 MMbbl/day in 2005. Driven by the exploitation of tight sand formations, the United States remained the world's top producer of petroleum and natural gas hydrocarbons in 2015.[10] Shale oil is playing a significant role in the global energy industry, and a worldwide shale-oil boom is predicted.[11−13]

Preliminary evaluation has shown that shale oil resources are very rich in China, with the amount of geological resources put at 32 billion barrels, and China ranked third among the 41 countries, which have an accumulated total shale oil resource of 345 billion barrels.[14] At present, in China, a number of reserves in which the amount of geological resources are between 3.5×10^9 and 7×10^9 barrels have been discovered (for example, in the Triassic Yanchang Formation of the Erdos Basin, Permian Lucaogou Formation of the Junggar Basin, and the Qingshankou Formation of the Songliao Basin). There are also many important discoveries in the lime-shale of Bohai Bay area and in the Sichuan Basin.[15,16] Compared with marine shale oil in North America, the lacustrine shale oil in China is heavier and has higher amounts of polar components; resin and asphaltene is much more abundant than in the North America reservoirs. The presence of these components in the lacustrine shale oil is thought to result in stronger adsorption of oil within the pores of the shale system, which requires extra effort to remove and makes the reservoir more difficult to develop. These polar components should be accounted for in the assessment of shale oil production in China because they strongly interact with kerogen, minerals, and the widespread nanopores in the shale rock,[17−19] leading to errors in recoverable resource estimation.

The adsorption of alkanes on carbonaceous materials, akin to the kerogen, has been studied in recent years. McGonigal et al.

Received: September 16, 2017
Revised: December 7, 2017
Published: December 18, 2017

DOI: 10.1021/acs.energyfuels.7b02763
Energy Fuels 2018, 32, 1155−1165

directly imaged a two-dimensional, high-degree ordering of the alkane layer at the liquid/graphite interface using a scanning tunneling microscope (STM).[20] Castro et al. reported that longer alkanes show a strong preference for adsorption onto graphite.[21] Furthermore, Severson and Snurr studied the adsorption isotherms of linear alkanes (ethane, pentane, decane, and pentadecane) on activated carbon and evaluated the functions of pore size, chain length, and temperature on adsorption.[22] Recently, Harrison et al. studied the single component preferential adsorption of linear and branched alkanes in pores with different apertures (1, 2, and 4 nm) at 390 K.[23]

A similar issue of accounting for hydrocarbons trapped in narrow pores for shale gas has been discussed by Ambrose et al., who suggested that an adjustment of adsorption-phase volume is necessary for gas-in-place (GIP) calculations, leading to a 10 to 25% decrease in GIP in comparison to the conventional method for assessment.[24−26] In addition, Wang reported that the unrecoverable fraction of oil-in-place (OIP) is 13% in Bakken shale[27] when the adsorption of alkanes in a graphite model is taken into consideration. Nevertheless, there are relatively few studies that explore the effect of polar component adsorption on the estimation of shale oil-in-place.

While the interaction of hydrocarbon molecules with pores and surfaces coated with kerogen-like materials has been more extensively studied, shale consists of two parts: organic matter (kerogen) and inorganic matter (minerals). The inorganic part of shale mainly contains quartz, calcite, feldspar, and clay minerals. Each kind of mineral makes up a certain volume fraction of a lacustrine and marine shale and plays an important role in shale systems through presenting intra- and interparticle pore networks that may hold hydrocarbons. Studying the interface of inorganic pores with oil is challenging, and computational chemistry simulations offer great potential to examine the properties of mineral interfaces and oil mixtures at an atomistic level. Previous simulation studies of mineral-organic interfaces have been widespread and extensively studied in the past, such as quartz,[28−30] calcite,[31] montmorillonite,[32] kaolinite,[33] and muscovite.[34]

Kaolinite often forms surface coatings in the inorganic pores of shale reservoirs as well as forming pore-filling aggregates and presents interparticle and intraparticle pore surfaces. Kaolinite is different from certain other clay minerals such as illite, smectite, and chlorite due to the octahedral−tetrahedral structure presenting two different surfaces, the mainly oil-wetting silicate surface, and the water-wetting aluminol surface. A significant number of computational studies have been published on kaolinite surfaces,[33,35−44] but these have primarily focused on the adsorption mechanisms of either a single molecule or a relatively small number of organic molecules to the mineral. Because shale oil contains different types and molecular-weight alkanes, aromatic hydrocarbons, and polar compounds, it is important to study the adsorption of different alkanes in the presence of aromatic and polar compounds to build a more-complete picture of the mineral−oil interface. In addition, temperature and pressure change with depth and maturity in a shale reservoir; therefore, it is also important to take these into consideration when considering shale oil adsorption.

In this present study, the adsorption behavior of a simple six-component model crude oil mixture on kaolinite basal surfaces (to represent a shale component) was studied under reservoir conditions using molecular dynamics (MD) simulations. The main objectives were (1) to provide nanoscale molecular-level resolution for studying the interactions at the hydrocarbon−shale interface, (2) to accurately characterize the adsorption properties of alkanes and polar compounds in the mineral slit-shaped pore space under different temperatures and pressures, and (3) to provide improved parameters for the calculation of the unrecoverable fraction for shale OIP estimation.

2. MODELS AND SIMULATION DETAILS

The kaolinite unit cell has the chemical formula $Al_2Si_2O_5(OH)_4$, without isomorphic substitutions. The initial atomic positions were taken from the American Mineralogist Crystal Structure Database (AMCSD).[45,46] This was converted to a cubic cell. The model contained three periodically replicated sheets of kaolinite, creating a clay slab of 252 unit cells (12 × 7 × 3), as shown in Figure 1g, with dimensions of approximately 6.2 × 6.3 × 1.9 nm. The kaolinite structures initially occupied the region $0 < z < 1.9$ nm in all models, and the clay mineral position varied slightly over all time scales modeled. Curtis et al. reported that a large number of nanoscale pores appeared when R_o (reflectance of vitrinite; this reflects the maturity of the shale) is higher than 0.9%.[47] Pores having a size under 20 nm play an important role in the shale systems,[48] and the 8 nm slit-shaped pore (or gallery) in the present model was built to represent these pores.

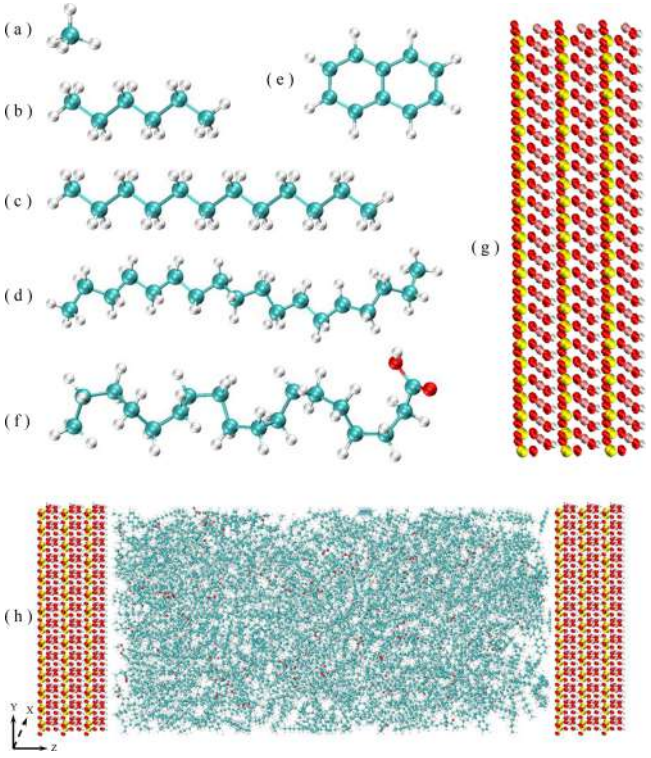

Figure 1. Molecules in the oil mixture: (a) methane (CH_4), (b) *n*-hexane (C_6H_{14}), (c) *n*-dodecane ($C_{12}H_{26}$), (d) *n*-octadecane ($C_{18}H_{38}$), (e) naphthalene ($C_{10}H_8$), (f) octadecanoic acid ($C_{18}H_{36}O_2$), (g) kaolinite surfaces, and (h) starting configuration of oil mixture in the kaolinite nanopore.

A mixture of methane (CH_4), *n*-hexane (C_6H_{14}), *n*-dodecane ($C_{12}H_{26}$), *n*-octadecane ($C_{18}H_{38}$), naphthalene ($C_{10}H_8$), and octadecanoic acid ($C_{18}H_{36}O_2$) represented the oil mixture molecules in these simulations (Figure 1a-f). The possible adsorption mechanisms of fatty acids on aluminol surface have

DOI: 10.1021/acs.energyfuels.7b02763
Energy Fuels 2018, 32, 1155−1165

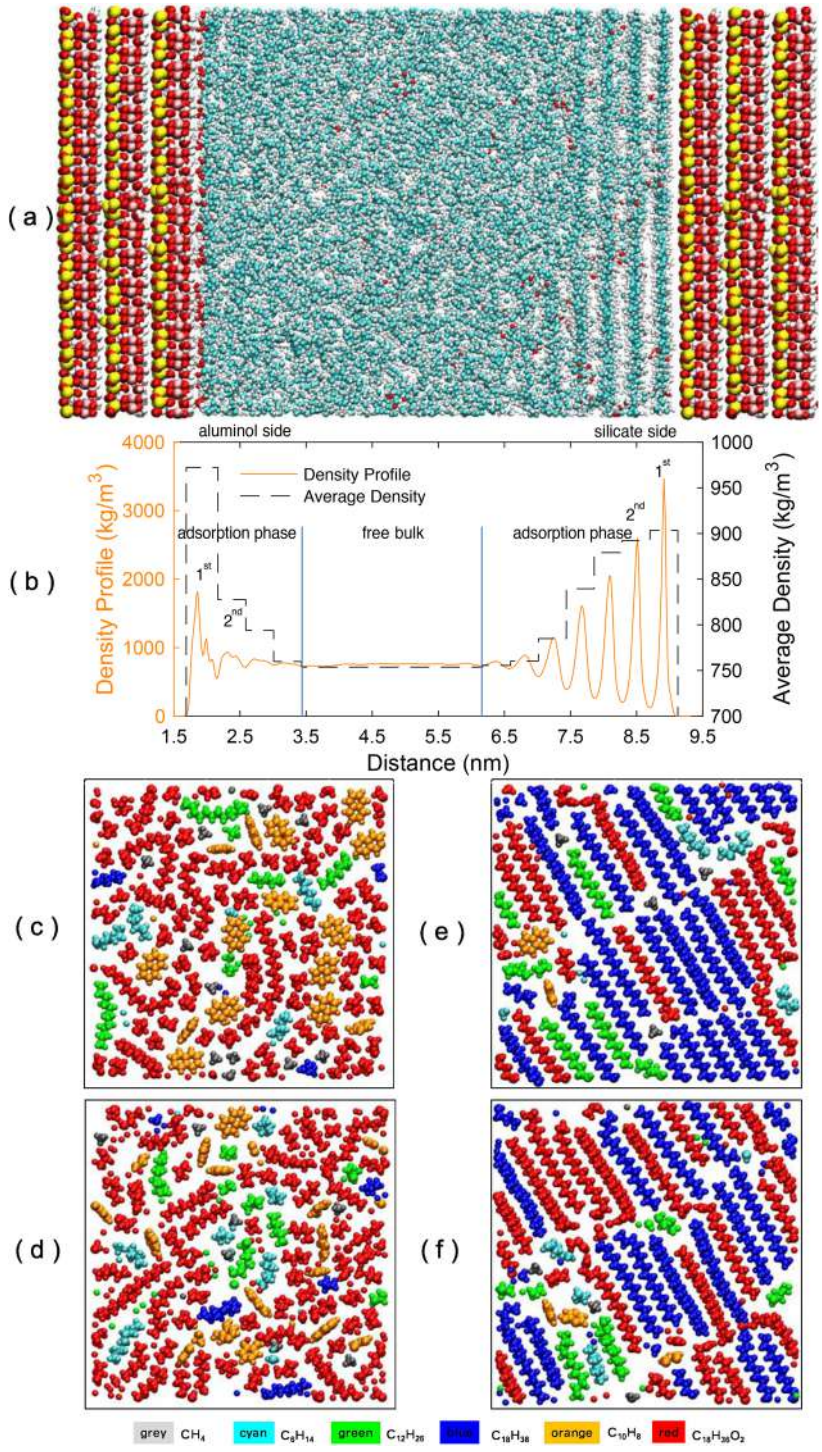

Figure 2. Adsorption of the 6-component oil mixture in a 7.82 nm kaolinite pore (323 K, 100 bar) showing (a) a snapshot of the final frame of the simulation, (b) mass-density profiles across the pore, (c) a cross-section snapshot showing the first adsorption layer on the aluminol surface, (d) a cross-section snapshot showing the second adsorption layer on the aluminol surface, (e) a cross-section snapshot showing the first adsorption layer on the silicate surface, and (f) a cross-section snapshot showing the second adsorption layer on the silicate surface.

been previously studied in the literature and are mainly caused by hydrogen bonding and van der Waals interactions in the anhydrous condition.[49] While classical MD simulation is a powerful technique for understanding the interface structure and dynamics on models of sufficient size to obtain a reasonable degree of complexity, owing to the electronic structure not being included, it cannot be used to predict reactivity. Studies have previously been undertaken looking at reactions of fatty acids at clay mineral interfaces using electronic structure calculations but on far-smaller and less-complex model systems.[50] Classical MD can be used to simulate the formation of prereactions configurations and give an indicator of potential reactivity; however, this was not undertaken for the present work.[51]

To compare the adsorption characteristics of multiple components, 150 organic molecules were loaded for each

DOI: 10.1021/acs.energyfuels.7b02763
Energy Fuels 2018, 32, 1155−1165

component in the models, with the initial percentage of each component at 16.67% by number. Methane molecules were used to represent gas dissolved in the shale oil (C_1−C_5 fraction), *n*-hexane, and *n*-dodecane molecules for the low-carbon-number alkanes (C_6−C_{14} saturated hydrocarbon), *n*-octadecane molecules for high-carbon-number alkanes (C_{15+} saturated hydrocarbon), naphthalene molecules for aromatic hydrocarbons (C_{6+} aromatic hydrocarbon), and octadecanoic acid molecules for polar compounds (resin and asphaltene). The adsorbed molecules were inserted using the program PackMol,[52] resulting in the system presented in Figure 1h.

The ClayFF force field and the CHARMM36/CGenFF force field were used to model the kaolinite clay mineral basal surfaces and the organic oil molecules, respectively, within the simulations.[53−56] Both of these two force fields have recently been tested in conjunction, and the interacting properties between hydrated mineral surfaces and organic molecules can be accurately reproduced using ClayFF and CHARMM36/CGenFF force field.[57] Previous simulations have shown that the adsorption of organic molecules (which were parametrized with CHARMM/CGenFF) on quartz surfaces (which were parametrized with ClayFF) are consistent with not only ab initio molecular dynamics but also with experimental X-ray reflectivity data.[58] Intermolecular organic−clay mineral interactions were modeled using Lorentz−Berthelot mixing rules.

All simulations were performed using the MD suite GROMACS 4.6.7.[59,60] Real-space particle-mesh Ewald (PME) electrostatics and a van der Waals cutoff of 1.4 nm were used in all simulations. The parameters used in energy minimization and equilibration period were the same as Underwood et al.[33] This equilibration simulation was followed by a 200 ns production run in the NPT ensemble using a velocity-rescale thermostat with a temperature coupling constant of 1 ps and a semi-isotropic Parrinello−Rahman barostat with a pressure coupling constant of 1 ps. The simulations were run under several conditions: (1) a pressure of 100 bar and a temperature of 323 K, which represents the geological conditions of the Nenjiang Formation in Songliao Basin,[61] and (2) three more temperature points (298, 348, and 373 K at 100 bar) and three more pressure points (1, 50, and 200 bar at 348 K) were set to study the influence of temperature and pressure on the oil adsorption for the temperatures and pressures reflect the main distribution of the oil-window stage in the Nenjiang Formation.

All simulation trajectories have been captured using VMD 1.9.2.[62] The color scheme of all snapshots is defined as follows. The clay structure contains silicon (yellow), oxygen (red), aluminum (pink), and hydrogen (white) atoms. Organic molecules contain carbon (cyan), hydrogen (white), and oxygen (red). The atomic and molecular densities of the oil mixture across the nanopore were calculated using the analysis tools within GROMACS 4.6.7 and subsequently plotted using Matlab 2017. Owing to some of the simulations only reaching equilibrium at 140 ns (see the determination of equilibrium in the Supporting Information) to increase the statistics of the simulations, the simulation time was extended to 200 ns, and the last 60 ns was selected to calculate the density profiles and undertake analysis of oil partitioning. Full details of the analysis of the model oil partitioning are given in the Supporting Information.

3. RESULTS AND DISCUSSION

3.1. Volume and Density of Adsorption of Oil-Phase Molecules. To gain insight into the adsorption behavior of the six-component oil mixture molecules confined in the kaolinite nanopore, which consists of opposing silicate and aluminol surfaces, local density distributions, and configurations of different components after equilibration were collected for oil mixtures within a 7.82 nm interlayer (representing the nanopore space between the kaolinite sheets) at 323 K and 100 bar (Figure 2). The continuous mass density profile (collected by partitioning the simulation box into layers of 0.015 nm) normal to the kaolinite surface was calculated using the final 60 ns of simulation data and the last frame of the production model was captured as a snapshot to show the oil mixture distribution in region between the kaolinite sheets (Figure 2a). Figure 2b shows that the oil mixture molecules are not uniformly distributed throughout the slit-shaped pore, and the density is not symmetrical about the center line of the two interfaces. Owing to the strong intermolecular affinities between the kaolinite mineral sheets and the alkanes, increased order of the oil components through layering is evident in the mass density near the mineral interface, and the magnitude of the ordered arrangement gradually reduces with increasing distance from the aluminol and silicate surfaces, which varies depending on the nature of the molecule. In the bulk region, the computed mass density remains almost constant. The first density peak adjacent to the aluminol surface is 1887 kg/m^3, which is approximately 1.5 times greater than that of the bulk fluid (764 kg/m^3); on the opposite side, the first density peak adjacent to the silicate surface is 3404 kg/m^3, which is approximately 3.5 times greater than that of the bulk fluid. Such a high density is due to the increased order in the close packed two-dimensional layers, making it into a relatively immobile solid-like state.[27,63] Away from the kaolinite interface region, surface induced structuring contributes a diminishing influence on the mass density, thus leading to a lower density peak of 999 kg/m^3 on the aluminol surface and 2519 kg/m^3 on the silicate surface. In the slit-shaped pore midplane, the physical properties of the bulk fluid show no strong fluctuations.

With the objective of determining an improved estimate of the recoverable oil-in-place, the volume occupied by the adsorption phase, which exists in a solid-like state, must be determined and deducted from the total pore space. The mass density profiles of the oil mixture in the kaolinite model (Figure 2a,b) reveal the adsorption region, defined as the region in which their local density deviates from the bulk value.[63−65] Recent studies of liquid structure theory modeling for non-attractive hard spheres also show pronounced oscillations in the density close to a boundary surface, with Davidchack et al. showing these oscillations are caused by the surface providing a translational plane rather than the molecules adhering to the surface.[66] Although density oscillations are found in liquid structure models with no attractive potential between the surface and the molecules, the average density of the "oscillation" region at the boundary is almost the same as that in the bulk region. The average density of each adsorption layer was also calculated for the kaolinite pore and analyzed (eq S1). The result shows that average density of oil mixture in the adsorption region is significantly greater than that in the bulk region (Figure 2b), evidencing adsorption on the surface. The oil mixture contains four adsorption layers on the aluminol surface and seven on the silicate surface, indicating differential multilayer adsorption of oil mixture molecules on the surface of kaolinite sheets. The solvation forces between *n*-alkanes and mica surfaces, measured by Christenson et al.,[67] showed decaying layered structuring, and the interlayer spacing

DOI: 10.1021/acs.energyfuels.7b02763
Energy Fuels 2018, 32, 1155−1165

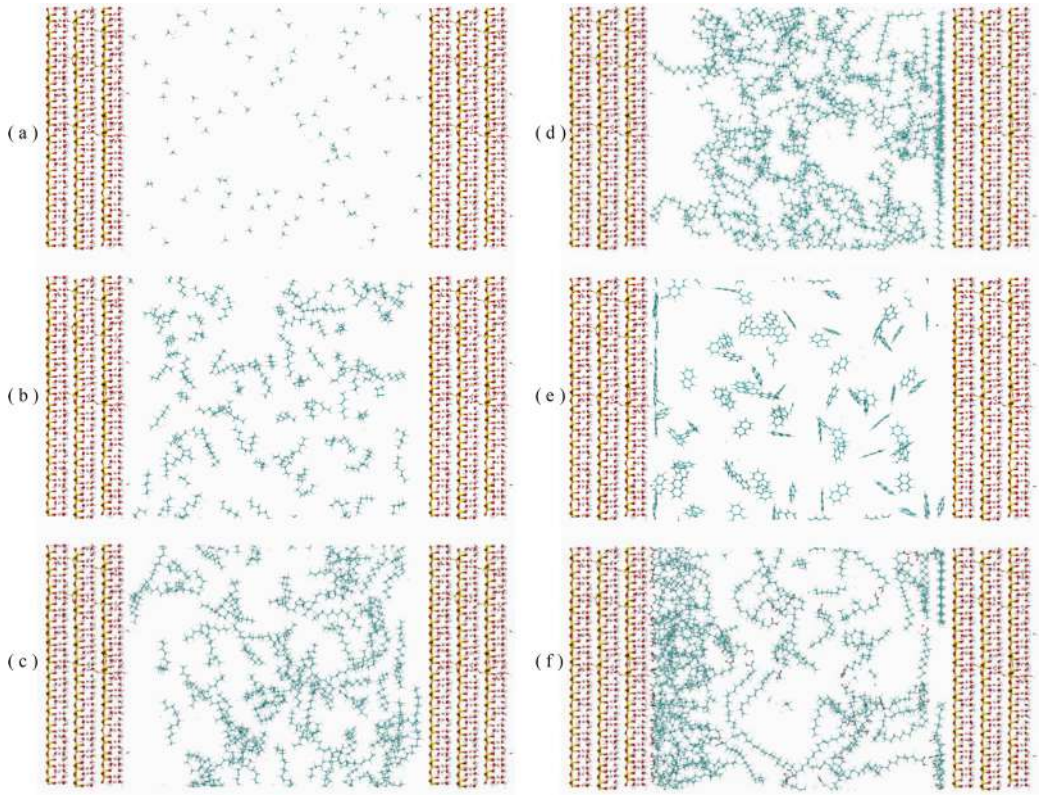

Figure 3. Snapshot showing the adsorption characteristics of each of the 6 oil components in a 7.82 nm kaolinite slit-shaped pore at 323 K and 100 bar: (a) methane, (b) *n*-hexane, (c) *n*-dodecane, (d) *n*-octadecane, (e) naphthalene, and (f) octadecanoic acid.

observed (0.40−0.50 nm) was approximately equal to the width of alkane molecules while independent of the chain length (1.35 nm for *n*-octane). Our analysis shows that the layer thickness is ∼0.44 nm on the aluminol surface and ∼0.42 nm on the silicate surface (Figure 2b), in good agreement with the above experimental results. Figure 2b also shows that the fluctuation of mass density extends 1.77 and 2.96 nm for the aluminol surface and silicate surfaces, respectively, suggesting that, under these conditions and for a 7.82 nm pore with kaolinite surfaces, the adsorbed hydrocarbon phase accounts for 60.4% of the pore volume. The adsorption-phase mass-transfer ratio (eq S2) in the 8 nm kaolinite mineral pore is 65.7% in the kaolinite pore. The $C_{ada\text{-}a}$ and $C_{ads\text{-}a}$ of the aluminol and silicate surfaces are, respectively, calculated as 1.44 and 2.47 mg/m^2 (through eqs S3 and S4). For the model oil studied, the adsorption capacity of the silicate surface is much greater than that of the aluminol surface.

Additionally, to investigate the oil mixture adsorption characteristics on kaolinite surfaces, in-plane cross-section images are taken to show the first and second adsorption layer on both the aluminol and silicate surfaces (Figure 2c−f). In the first adsorption layer on the aluminol mineral interface, octadecanoic acid and naphthalene occupy most of the surface area and are distributed with no apparent order (Figure 2c), as in the second adsorption layer (Figure 2d). In comparison to the aluminol surface, on the silicate surface, the octadecanoic acid and *n*-octadecane are distributed in an ordered manner, with a 30° angle between the *n*-octadecane molecules long axis and the crystallographic *y* direction, shown as a blue dashed line in Figure 2e, which is determined by the crystal lattice symmetry. As a comparison, Dirand et al. found that the distance between *n*-octadecane molecules between planes in the crystal structure of *n*-octadecane is 0.48 nm,[68] which is 0.03 nm larger than that observed on the silicate surface. This indicates that *n*-octadecane molecules arrange closer due to the hexagonal lattice of the silicate side. However, the thickness in the crystallographic *z* direction is 0.40 nm, which is 0.04 nm smaller than that on the silicate surface. That is because the temperature in this simulation is 323 K, which is 30 K higher than the *n*-octadecane crystallization temperature. Even though the *n*-octadecane molecules are attracted toward the silicate surface, temperature plays an important role in the adsorption characteristics. The *n*-octadecane molecules formed in a more crystal-like state but still contain molecular gauche conformers and torsion of the chains of alkanes. As such, the thickness of one adsorption layer is larger than the thickness of a similar layer of crystalline *n*-octadecane.[68] Small molecules (methane, *n*-hexane, and naphthalene) are arranged in the interstices formed between the regions occupied by *n*-octadecane and octadecanoic acid. This suggests that some molecular-sized nanoporosity is formed by the imperfect packing of larger organic molecules on the mineral surface. The model oil molecules in the second adsorption layer on the silicate surface are more disordered than the first adsorption layer, as evidenced by the increased distance between them and the silicate surface (Figure 2f).

3.2. Comparison of the Adsorption Characteristics of Multiple Components on Both Surfaces of Kaolinite. Here, the adsorption character and mole number density of each component in the six-component oil mixture on kaolinite surfaces are discussed. First, a snapshot of the last frame of oil mixture adsorption simulation is taken to show the qualitative evaluation of each component adsorption character of the oil mixture in the kaolinite model (Figure 3). Each component is

DOI: 10.1021/acs.energyfuels.7b02763
Energy Fuels 2018, 32, 1155−1165

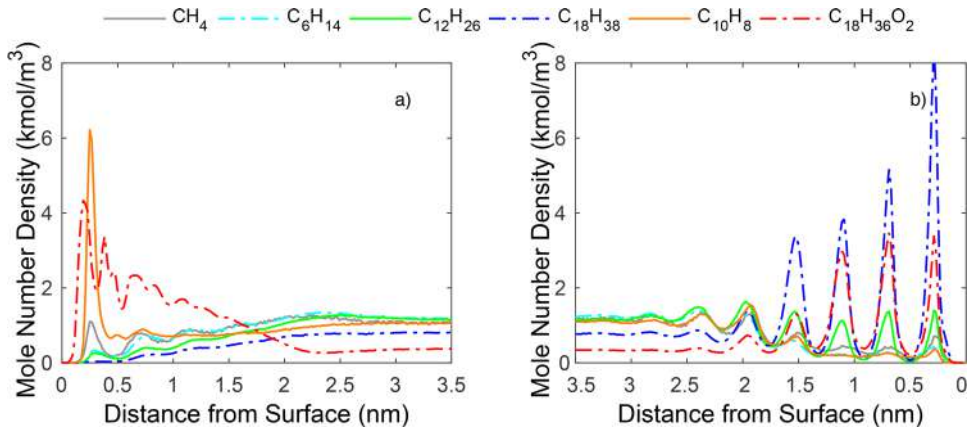

Figure 4. Analysis of the mole number density profiles of the six oil components on (a) the aluminol surface and (b) the silicate surface.

displayed separately on Figure 3a–f. We can see from Figure 3a that methane is mainly distributed evenly in the kaolinite slit-shaped pore. Figure 3b shows that *n*-hexane has little affinity for either surface of the kaolinite but is still evenly distributed throughout the slit-shaped pore. However, the long alkanes, *n*-dodecane and *n*-octadecane, are more likely to be adsorbed on the silicate surface (Figure 3c,d). The majority of the *n*-octadecane are observed on the silicate surface in the first adsorption layer. In contrast, naphthalene and octadecanoic acid have a higher probability of being adsorbed on the aluminol surface. This is due to the attractive forces between the conjugated π-system of naphthalene and the slightly positively charged hydrogen atoms of the kaolinite aluminol surface, as well as the polar interactions and hydrogen bonding between the carboxylate groups and the hydroxyl groups for octadecanoic acid (Figure 3e,f).

Mole number density profiles of each component in the oil mixture were calculated to evaluate the adsorption characteristics quantitatively using eq S9 (Figure 4a,b). The mole number density profile of methane shows four distinct adsorption layers on the aluminol surface, and the first adsorption layer peak value is a little higher than that of bulk (Figure 4a). The thickness of each monolayer is 0.42 nm, by which the mole number density profile is determined. In contrast to the aluminol surface, the mole number density profile of methane on the silicate surface shows seven distinct adsorption layers, but most are lower than the pore center region (Figure 4b). This phenomenon is not like the single-component methane adsorption characteristics on the Na–montmorillonite surface, which has only one major adsorption layer, in which the density value is almost 4 times greater than that of bulk methane,[69] owing to the existence of the other oil components. The methane molecules are not only adsorbed on the mineral surface but also become dissolved in the oil mixture.

The adsorption mole number density profiles of liquid hydrocarbons (*n*-hexane, *n*-dodecane, and *n*-octadecane) on the aluminol surface show that there are also four adsorption layers (Figure 4a), as for methane. Also, the density values of the adsorption layers are lower than in the bulk (slit-shaped pore middle) region, indicating that the liquid hydrocarbons are less likely to adsorb on the aluminol surface. In contrast, there are seven adsorption layers of liquid hydrocarbons on the silicate surface, and the density values are much higher than in the bulk region. This is especially the case for the longer *n*-octadecane molecules, which occupy almost half of the first adsorption layer's available surface area at the interface. Within the first four adsorption layers on the silicate surface, which is the region most influenced by the kaolinite sheet, the values of the mole number density profiles peaks were found to decrease with the alkane chain length ($\rho_{\text{mol-}C_6H_{14}} < \rho_{\text{mol-}C_{12}H_{26}} < \rho_{\text{mol-}C_{18}H_{38}}$), as shown in Figure 4b.

The aromatic hydrocarbon (naphthalene) mainly adsorbs directly onto the aluminol surface and not on the silicate surface, as indicated by a single prominent near surface peak in the density profile at the aluminol interface (Figure 4a), with a value of 6.20 kmol/m^3, which is over 6 times greater than the bulk density (0.87 kmol/m^3). Although there are seven adsorption layers on the silicate surface, the density values of each are much lower than that of the bulk (Figure 4b), which is in accord with the snapshot showing the adsorption characteristics of the individual component in Figure 3e. This indicates that the naphthalene adsorption capacity on, and interactions with, the aluminol surface are much higher than on the silicate surface.

The density profile for the adsorption of the polar octadecanoic acid (Figure 4a,b) showed three adsorption layers on the aluminol surface and six layers on the silicate surface. The density of octadecanoic acid in the bulk region is the lowest, indicating that octadecanoic acid is likely to be adsorbed the most, compared with the other oil components. There are two distinct peaks in the octadecanoic acid density in the first adsorption layer on the aluminol surface, which is different from the other oil components. The headgroup (carboxylate group) of the octadecanoic acid molecule is adsorbed on the aluminol surface, with hydrogen bonding to the Al–OH groups partly suggested by the visual analysis, as can be observed in in Figure 3f. This results in the hydrophobic alkyl chain orienting away from the surface. This can be contrasted with the silicate interface, where the alkyl chain can be observed bonded on and parallel to the kaolinite mineral surface, with the carboxylate headgroup oriented away from the surface. These results are consistent with the work of Underwood et al.[33] On the silicate surface, the octadecanoic acid molecules are adsorbed with an almost parallel orientation to the silicate surface with a gauche conformation similar to the *n*-octadecane molecules. The octadecanoic acid forms only one peak in the first adsorption layer, with five density peaks having values higher than that of the midplane (bulk) region, and the density of the first layer is not higher than that of the second layer, owing to the competitive adsorption of *n*-octadecane.

DOI: 10.1021/acs.energyfuels.7b02763
Energy Fuels 2018, 32, 1155–1165

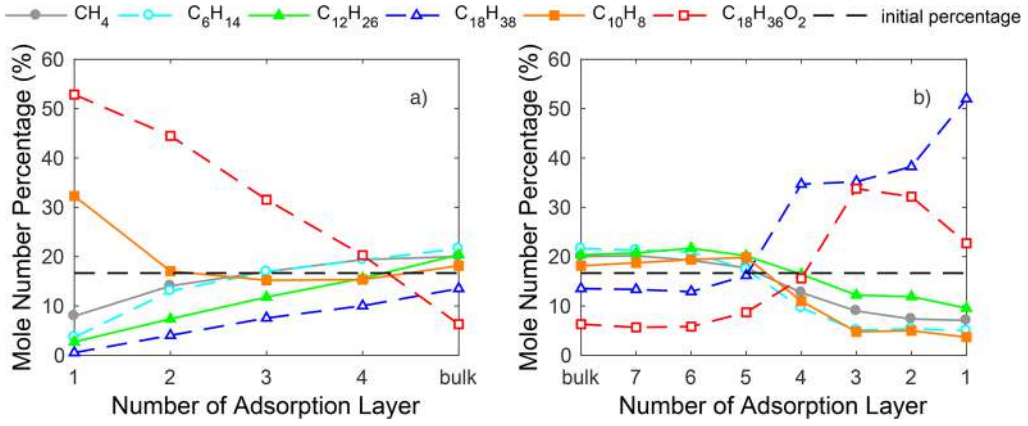

Figure 5. Mole number percentage of the six oil components on (a) the aluminol surface and (b) the silicate surface.

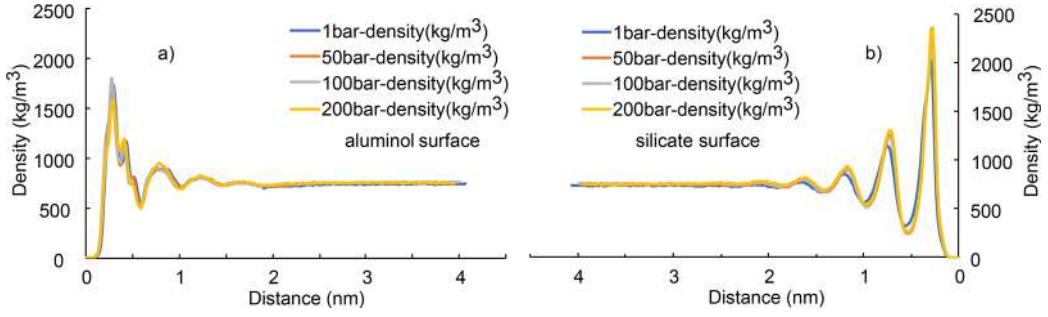

Figure 6. Mass density profiles for oil mixture at different pressures on kaolinite surface: (a) the aluminol surface and (b) the silicate surface.

Additionally, to compare the adsorption characteristics of the six components, the adsorption percentage of each individual component in the different adsorption layers was calculated (eq S10). Mole number percentage of six components on the aluminol side shows that naphthalene and octadecanoic acid occupy almost 85% of first adsorption layer (Figure 5a). Both of these molecules follow the trend that adsorption percentage decreases with the number of adsorption layers (this phenomenon can be called a positive adsorption trend). However, the alkanes have a contrary trend (this phenomenon can be called a negative adsorption trend), and furthermore, the adsorption percentage of each component in the four adsorption layers decreases as the carbon number increases.

On the silicate surface, *n*-octadecane has a trend that adsorption percentages decrease with the number of adsorption layers, which is different from the trend on the aluminol surface, indicating *n*-octadecane is more likely to be adsorbed on the silicate surface (Figure 5b). Adsorption percentages of methane, *n*-hexane, and *n*-dodecane increase with the number of adsorption layers, the same trend as on the aluminol surface, indicating they are less likely to be adsorbed on both surfaces of kaolinite compared with the other three components. Naphthalene also has a negative adsorption trend on the silicate surfaces, similar to methane, *n*-hexane, and *n*-dodecane, which is different from the trend on the aluminol surface, and it indicates that naphthalene is likely to be adsorbed preferentially on aluminol surfaces. Meanwhile, the adsorption percentage of each liquid alkane component (*n*-hexane, *n*-dodecane, and *n*-octadecane) in the first four adsorption layers increases with increasing number of carbon atoms in the chain.

After comparison of the adsorption character and mole number density profile of the six components in the oil mixture on kaolinite surfaces, it can be concluded that (1) the number of adsorption layers, density of each adsorption layer and total adsorption capability on the aluminol surface are all smaller than those on the silicate surface; (2) the surface lattice structure of the silicate surface guides the arrangement of oil molecules, whereas the aluminol surface does not; (3) aromatic naphthalene and polar octadecanoic acid molecules are more likely adsorbed on the aluminol surface, while *n*-octadecane molecules are more likely to be found adsorbed on the silicate surface (meanwhile, the percentage of alkane molecules in the adsorption layers on the silicate surface increases as the number of carbon atoms increases); (4) alkanes have a negative adsorption trend on aluminol surfaces, and naphthalene and octadecanoic acid have a positive adsorption trend; and (5) the *n*-octadecane molecules have a positive adsorption trend. Meanwhile methane, *n*-hexane, *n*-dodecane, and naphthalene have a negative adsorption trend on the silicate surface. This partitioning is important as oil mixture components' adsorption characteristics play an important role in determining the surface tension and nanoscale flow mechanism of the oil in the pores. Additionally, this principle can also be applied to light hydrocarbon recovery in shale oil recovery evaluation and enhanced oil recovery more generally.

3.3. Effect of Pressure on Oil Mixture Adsorption. In this section, we discuss the influence of pressure on the adsorption characteristics of the multiple oil components. Mass density profiles of the oil mixture at four different pressure points (1, 50, 100, and 200 bar) are imaged on both sides of the kaolinite slit-shaped pore (Figure 6a,b). First, the thickness of the adsorption layer extends very slightly with the increase of pressure. Meanwhile, as the pressure rises, the number of adsorption layers remains the same on both surfaces of the kaolinite sheets (four layers on the aluminol surface and five layers on the silicate surface). In addition, the density of the oil

DOI: 10.1021/acs.energyfuels.7b02763
Energy Fuels 2018, 32, 1155−1165

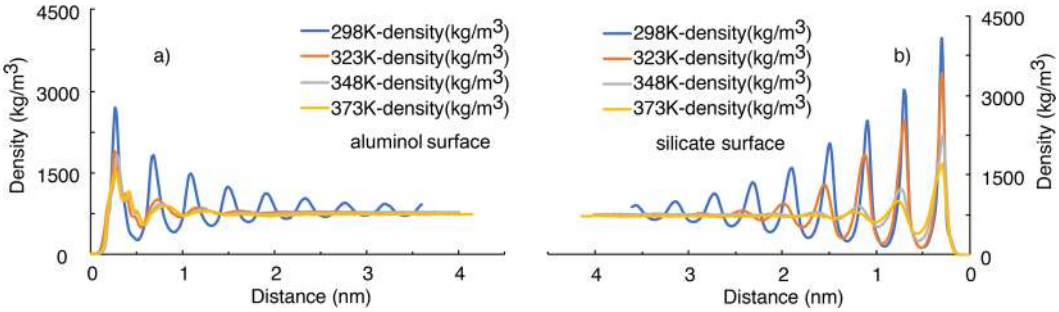

Figure 7. Mass-density profiles for oil mixture at different temperatures on the kaolinite surface: (a) the aluminol surface and (b) the silicate surface.

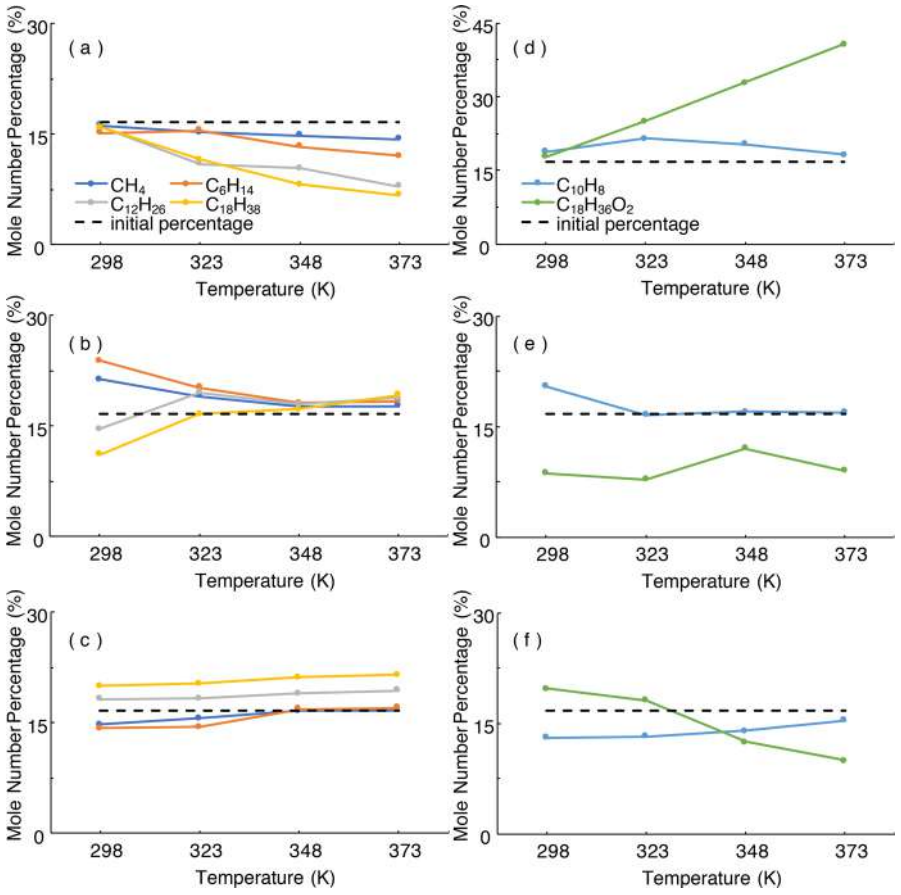

Figure 8. Mole-number percentage of six components at different temperatures in kaolinite sheets: (a) alkanes on the aluminol side, (b) alkanes in the bulk region, (c) alkanes on the silicate side, (d) naphthalene and octadecanoic acid on the aluminol side, (e) naphthalene and octadecanoic acid in the bulk region, and (f) naphthalene and octadecanoic acid on the silicate side.

mixture has small changes with pressure and the thickness of adsorption layers decreases slightly with pressure on silicate surfaces. This is because as the pressure increases, the force exerted on the system increases and this will lead to closer packing of the oil molecules. Therefore, the density peak has a slight increase, commensurate with a decrease in the thickness of the initial layer, although, overall, pressure appears to have only a small effect.

3.4. Effect of Temperature on Six-Component Oil Mixture Adsorption. In this section, the influence of temperature on the adsorption characteristics of the six components of the oil mixture is studied. The mass densities at four different temperatures (298, 323, 348, and 373 K) were plotted for both basal surfaces of the kaolinite model (shown in Figure 7a,b). The mass density profiles start from the surface of the kaolinite sheets and end in the midpoint of the oil mixture in which more bulk-like behavior is expected. First, we can see that the lengths of the profiles extend with the increase of temperature, i.e., the bulk density of the oil mixture decrease with increased temperature. It can also be noted that, as the temperature rises, the number of adsorption layers on the aluminol surface drops from six to three (6 layers at 298 K, 4 at 323 K, 4 at 348 K, and 3 at 373 K), and on the silicate surface it drops from 7 to 5 (7 layers at 298 and 323 K and 5 at 348 and 373 K). Although the thickness of each adsorption layer increases with temperature, the mass density, the total thickness of the adsorbed layer and the total adsorption capability have different trends on the opposing sides of the kaolinite pore, with the silicate and aluminol layers showing distinct behaviors. It is notable that each mass-density peak maxima of the

DOI: 10.1021/acs.energyfuels.7b02763
Energy Fuels 2018, 32, 1155−1165

adsorption layers moves further from the surface of the kaolinite with increased temperature (the position of second density peak maxima on the silicate surface: 0.69 nm at 298 K, 0.69 nm at 323 K, 0.74 nm at 348 K, and 0.78 nm at 373 K), with the exception of the first-adsorption-layer peak maxima (the position of first density peak maxima on the silicate surface is almost 0.29 nm at all four temperature points), where the change is negligible. This indicates that, independent of the temperature, the arrangements of the oil mixture components and the mass center of the first adsorption layer are almost the same, with small changes caused by the gauche conformers and torsion of the chains of alkanes and octadecanoic acid. It can also be noticed that there is only a single peak maxima in the first adsorption layer on the aluminol surface at 323 K, which is different to the other three temperatures studied. This arises due to the arrangement of octadecanoic acid molecules on the aluminol surface at 323 K being the same as that on the silicate surface, where the molecules are adsorbed with in an almost parallel orientation to the aluminol surface, with a zigzag arrangement.

It is useful to compare the thickness of each adsorption layer on the silicate surface at the four temperatures, with the intermolecular plane packing thickness of *n*-octadecane in a crystalline state (293 K), which was measured by Dirand et al.[68] The thickness of each adsorption layer at the four temperatures is 0.41, 0.42, 0.43, and 0.44 nm in the *z* direction for 298, 323, 348, and 373 K, respectively. These are comparable to the 0.40 nm distances experimentally reported in crystalline *n*-octadecane at 293 K. The slight (under 10%) increase of these values arises from the fact that (1) with the increase of temperature, gauche conformations in the alkane chain are more common, as are the appearance of rotatory states due to thermal motion of the molecules; and (2) the oil mixture in this simulation contains several small molecules (such as methane and *n*-hexane) dissolved in the longer-chain molecules, which will lead to the increase of the adsorption layer thickness.

Additionally, to compare the adsorption characteristics of the six components at four temperatures quantitatively, the adsorption percentages of individual component in a defined adsorption region on both sides of the kaolinite sheets was calculated through eq S11. Plotted figures of the mole number percentage of the six components on the aluminol interface show that naphthalene and octadecanoic acid occupy almost 85% of space in the first adsorption layer. Figure 8a–c shows the mole number percentage of alkanes (methane, *n*-hexane, *n*-dodecane, and *n*-octadecane) at the four different temperatures on the aluminol surface, the bulk region, and the silicate surface, respectively. Figure 8e,f show the same data for naphthalene and octadecanoic acid, at four different temperatures on the aluminol surface, in the bulk region and on the silicate surface, respectively. The black dashed line shows the initial percentage of each component in the kaolinite model (i.e., 16.67%). The mole number percentage of alkanes in the adsorption region on the aluminol surface decrease with the rise in temperature, and they are all lower than the initial percentage, which indicates that alkanes are not likely to be adsorbed on the aluminol surface. At lower temperature (298 K) the percentages of alkanes are almost the same as one another, and, as such, very near to the initial percentage; however, with the increase of temperature, the percentages of alkanes with a high carbon number in the interfacial region decrease faster than those alkanes with a low carbon number. At 373 K, the percentages of the alkanes are separated by the largest amount relative to each other. The order of percentages of alkanes on the aluminol surface is methane < *n*-hexane < *n*-dodecane < *n*-octadecane, which are 14.4%, 12.1%, 7.9%, and 6.8%, respectively (Figure 8a). When the percentage of octadecanoic acid on the aluminol side is considered, it has a regular linear growth trend with the increase in temperature. However, the naphthalene has a slightly decreasing trend. Furthermore, the percentages of both the octadecanoic acid and naphthalene are higher than the initial (16.6%) percentage, which indicate that they are more likely to be adsorbed on the aluminol surface than the alkanes (Figure 8d), and octadecanoic acid has the biggest percentage in the adsorption region on the aluminol side.

In this section, we discuss the adsorption percentage of six components on the silicate surface. Here, the alkanes have an opposite trend to that observed above on the aluminol surface, with increasing adsorption percentages as temperature increases. Alkanes with a high carbon number are adsorbed preferentially on the silicate surface than alkanes with a lower carbon number, which is again a different trend from that observed on the aluminol surface (Figure 8c). For the percentages of octadecanoic acid and naphthalene on the silicate side, octadecanoic acid decreases with increasing temperature. Naphthalene shows a slight increase in adsorption with temperature increase. Meanwhile, both molecules show relatively lower adsorbed amounts than the initial percentage, which indicates that they are less likely to be adsorbed on the silicate surface, especially at higher temperatures (Figure 8f).

Finally, we analyze the percentage of multiple components in the bulk region, which also reflects the percentage of total adsorption capacity on the different basal surfaces of the kaolinite sheets. At 298 K, the percentage of the alkanes with low carbon numbers (methane and *n*-hexane) are higher in the bulk region than longer alkanes; however, with increased temperature, the percentages of alkanes begin to converge, approaching the initial percentage. At 373 K, the order of alkane abundance in the bulk region is methane < *n*-hexane < *n*-dodecane < *n*-octadecane, which are 17.7%, 18.4%, 18.8%, and 19.2%, respectively (Figure 8b). This indicates that the alkanes with higher carbon number are more likely to be adsorbed on both surfaces of the kaolinite sheets at low temperature and become more mobile and release at high temperature. The change in distribution percentage of naphthalene in the bulk has the same trend as that of the alkanes with low carbon numbers, and it is almost the same as the initial percentage. This indicates that the percentage of naphthalene in the bulk region is the same with that in the near-surface region. Percentage analysis of the octadecanoic acid shows it does not have a definite trend; although as they are all less than the initial percentage, this indicates that octadecanoic acid molecules are adsorbed more on the surfaces overall.

4. CONCLUSIONS

In this work, we perform a study of the adsorption characteristics of a multicomponent oil mixture in a kaolinite nanoscale slit-shaped pore to represent intraparticle pores within a shale oil system. We discuss the total adsorption-phase thickness in the nanopore and the characteristics of each component. The main conclusions of the study are as follows.

(1) Under reservoir conditions (323 K and 100 bar), there are four distinct adsorption layers of oil components on aluminol surfaces and seven layers on silicate surfaces, and the thickness of each layer is 0.44 nm on the

DOI: 10.1021/acs.energyfuels.7b02763
Energy Fuels 2018, 32, 1155–1165

aluminol surface and 0.42 nm on the silicate surface. In addition, the adsorption capacity per unit area of aluminol and silicate surface is 1.44 and 2.47 mg/m^2, respectively. The silicate surface orders the arrangement of adsorbed molecules, and the adsorption capacity and density are higher than that of the aluminol surface.

(2) Naphthalene and octadecanoic acid are more likely to be adsorbed on the aluminol surface. Meanwhile, heavier hydrocarbons (*n*-octadecane) and octadecanoic acid are more likely to be adsorbed on the silicate surface. With the increase of carbon number, the adsorption percentages of the linear alkanes decrease in adsorption layers. In addition, alkanes have a "negative adsorption trend" on aluminol surface, while naphthalene and octadecanoic acid have a "positive adsorption trend". In contrast, the trend on silicate surfaces is opposite to that on aluminol surfaces.

(3) Pressure has little influence on the adsorption of the oil mixture. With the increase of temperature, the thickness, density of adsorption layer, number of adsorption layers, and total adsorption amount decrease on both surfaces of kaolinite sheets. On the aluminol surface, the percentage of polar compounds increase, while the presence of alkanes decreases with temperature. At higher temperatures (348 and 373 K), the percentage of alkanes decrease with carbon number. However, these trends on the silicate surface are opposite to those found on the aluminol surface. At lower temperatures, enthalpy-driven interactions are more important than entropic ones. This explains the varying adsorption of oil components on different kaolinite surfaces. At higher temperatures, entropy becomes more relevant, thus leading to reduction in surface selectivity.

The findings illustrate that in nanopores in oil and gas reservoirs, layers of strongly bound oil profoundly modify the available pore volume. Critically, the presence of different mineral surfaces can selectively remove different components of crude oil and this is likely to be particularly important when considering oil migration pathways and, in particular, when considering surface wetness modification in enhanced oil recovery. Given the recent increase in resolution in computer tomography and mineral/pore mapping capabilities,[70] this present study allows the properties of identified pores to be further explored. Future work will explore the effect of pH and surface defects on the surface adsorption characteristics of the model oil. Furthermore, the parameters obtained here allow us to explore further recovery models for shale oil systems.

■ ASSOCIATED CONTENT

Supporting Information

The Supporting Information is available free of charge on the ACS Publications website at DOI: 10.1021/acs.energyfuels.7b02763.

Additional details of the analysis of model oil properties and the equilibrium and stability of systems. (PDF)

■ AUTHOR INFORMATION

Corresponding Authors

*E-mail: lushuangfang@upc.edu.cn. Phone: +86-18661856596.
*E-mail: chris.greenwell@durham.ac.uk. Phone: +44-01913342324.

ORCID

Shansi Tian: 0000-0001-6828-4263
Shuangfang Lu: 0000-0002-0758-4075

Author Contributions

S.T. performed the molecular simulations and wrote the main manuscript. V.E. provided the Gromacs software training and the method for solving problems in the simulations and helped draft the manuscript. S.L. defined (supervisor in China) the statement of the problem. C.G. provided the main idea and helped draft the manuscript. S.L, H.X. (vice supervisor in China), and C.G. (supervisor in the United Kingdom) designed and supervised the project. T.U. helped discussion of the main idea, provided the mineral model in the simulations, and drafted the manuscript. F.Z., G.C., C.W., and R.Z. processed data and plotted figures. All authors reviewed the manuscript.

Notes

The authors declare no competing financial interest.

■ ACKNOWLEDGMENTS

This study was partly funded by the National Natural Science Foundation of China (grant nos. 41572122, 41330313, and 41672116), the National Science and Technology Major Project (grant nos. 2016ZX05004-001 and 2016ZX05007-003), the National Basic Research Program of China (973 Program) (grant no. 2014-CB239005), and the Graduate Innovation Fund of China University of Petroleum (grant no. YCXJ2016004). The first author also would like to acknowledge the China Scholarship Council (CSC) for its financial support for his living expenses at Durham University, UK as a visiting Ph.D. student. We gratefully acknowledge Prof. H. Chris Greenwell for providing the opportunity for S.T. to visit the Greenwell research group. H.C.G. thanks the Royal Society for funding via an Industry Fellowship, and H.C.G. and T.R.U. also acknowledge funding from BP.

■ REFERENCES

(1) Bowker, K. A. *AAPG Bull.* **2007**, *91*, 523−533.
(2) Jarvie, D. M.; Hill, R. J.; Ruble, T. E.; Pollastro, R. M. *AAPG Bull.* **2007**, *91*, 475−499.
(3) Ross, D. J. K.; Bustin, R. M. *AAPG Bull.* **2008**, *92*, 87−125.
(4) Zou, C. N.; Dong, D. Z.; Wang, S. J.; Li, J. Z.; Li, X. J.; Wang, Y.; Li, D. H.; Cheng, K. M. *Petroleum Exploration and Development.* **2010**, *37* (6), 641−653.
(5) Horsfield, B.; Schulz, H. M. *Mar. Pet. Geol.* **2012**, *31*, 1−2.
(6) Kinley, T. J.; Cook, L. W.; Breyer, J. A.; Jarvie, D. M.; Busbey, A. B. *AAPG Bull.* **2008**, *92*, 967−991.
(7) Kuhn, P. P.; di Primio, R.; Hill, R.; Lawrence, J. R.; Horsfield, B. *AAPG Bull.* **2012**, *96*, 1867−1897.
(8) Kirschbaum, M. A.; Mercier, T. J. *AAPG Bull.* **2013**, *97*, 899−921.
(9) EIA. Where Our National Energy Comes From. https://www.eia.gov/energy_in_brief/article/shale_in_the_united_states.cfm (accessed Sep. 2016).
(10) Doman, L. United States remains largest producer of petroleum and natural gas hydrocarbons. http://www.eia.gov/todayinenergy/detail.cfm?id=26352 (accessed Sep. 2016).
(11) EIA. How much shale (tight) oil is produced in the United States? https://www.eia.gov/tools/faqs/faq.php?id=847&t=6 (accessed Sep. 2016).
(12) Zhang, L.; Bao, Y.; Li, J.; Li, Z.; Zhu, R.; Zhang, J. *Petrol. Explor. Develop.* **2014**, *41* (6), 703−711.
(13) Zou, C.; Yang, Z.; Zhang, G.; Hou, L.; Zhu, R.; Tao, S.; Yuan, X.; Dong, D.; Wang, Y.; Guo, Q.; Wang, L.; Bi, H.; Li, D.; Wu, N. *Petrol. Explor. Develop.* **2014**, *41* (1), 14−30.
(14) EIA. World Shale Resource Assessments. http://www.eia.gov/analysis/studies/worldshalegas/ (accessed Sep. 2016).

DOI: 10.1021/acs.energyfuels.7b02763
Energy Fuels 2018, 32, 1155−1165

(15) Jia, C. Z.; Zheng, M.; Zhang, Y. F. *Acta Petrolei Sinica.* **2014**, *35*, 1−10.
(16) Zou, C. N.; Zhai, G. M.; Zhang, G. Y.; Wang, H. J.; Zhang, G. S.; Li, J. Z.; Wang, Z. M.; Wen, Z. X.; Ma, F.; Liang, Y.; et al. *Petroleum Exploration and Development* **2015**, *42* (1), 14−28.
(17) Nelson, P. H. *AAPG Bull.* **2009**, *93*, 329−340.
(18) Zou, C.; Yang, Z.; Cui, J.; Zhu, R.; Hou, L.; Tao, S.; Yuan, X.; Wu, S.; Lin, S.; Wang, L.; Bai, B.; Yao, J. *Petrol. Explor. Develop.* **2013**, *40* (1), 15−27.
(19) Tang, X.; Zhang, J.; Wang, X.; Yu, B.; Ding, W.; Xiong, J.; Yang, Y.; Wang, L.; Yang, C. *Int. J. Coal Geol.* **2014**, *128*, 32−46.
(20) McGonigal, G. C.; Bernhardt, R. H.; Thomson, D. J. *Appl. Phys. Lett.* **1990**, *57*, 28−30.
(21) Castro, M. A.; Clarke, S. M.; Inaba, A.; Arnold, T.; Thomas, R. K. *J. Phys. Chem. B* **1998**, *102* (51), 10528−10534.
(22) Severson, B. L.; Snurr, R. Q. *J. Chem. Phys.* **2007**, *126*, 134708.
(23) Harrison, A.; Cracknell, R. F.; Krueger-Venus, J.; Sarkisov, L. *Adsorption* **2014**, *20*, 427−437.
(24) Ambrose, R. J.; Hartman, R. C.; Akkutlu, I. Y. Multi-component sorbed phase considerations for Shale Gas-in-place Calculations. *Proc. Society of Petroleum Engineers* **2011**, 1 DOI: 10.2118/141416-MS.
(25) Ambrose, R. J.; Hartman, R. C.; Diaz-Campos, M.; Akkutlu, I. Y.; Sondergeld, C. H. *Society of Petroleum Engineers.* **2012**, *17*, 219−229.
(26) Hartman, R. C.; Ambrose, R. J.; Akkutlu, I. Y.; Clarkson, C. R. Shale Gas-in-Place Calculations Part II - Multicomponent Gas Adsorption Effects. *Proc. Society of Petroleum Engineers* **2011**, 1.
(27) Wang, S.; Feng, Q.; Javadpour, F.; Xia, T.; Li, Z. *Int. J. Coal Geol.* **2015**, *147*, 9−24.
(28) Zhong, J.; Wang, P.; Zhang, Y.; Yan, Y.; Hu, S.; Zhang, J. *Energy* **2013**, *59*, 295−300.
(29) Wu, G.; He, L.; Chen, D. *Chemosphere* **2013**, *92*, 1465−1471.
(30) Xiong, Y.; Cao, T.; Chen, Q.; Li, Z.; Yang, Y.; Xu, S.; Yuan, S.; Sjoblom, J.; Xu, Z. *J. Phys. Chem. C* **2017**, *121* (9), 5020−5028.
(31) Lu, G.; Zhang, X.; Shao, C.; Yang, H. *Pet. Sci.* **2009**, *6*, 76−81.
(32) Underwood, T.; Erastova, V.; Cubillas, P.; Greenwell, H. C. *J. Phys. Chem. C* **2015**, *119* (13), 7282−7294.
(33) Underwood, T.; Erastova, V.; Greenwell, H. C. *J. Phys. Chem. C* **2016**, *120* (21), 11433−11449.
(34) Li, X.; Bai, Y.; Sui, H.; He, L. *Energy Fuels* **2017**, *31* (2), 1174−1181.
(35) Wilson, M. J. *Clay Miner.* **1999**, *34*, 7−25.
(36) van Duin, A. C.; Larter, S. R. *Org. Geochem.* **2001**, *32*, 143−150.
(37) Hu, X. L.; Michaelides, A. *Surf. Sci.* **2008**, *602*, 960−974.
(38) Johnson, E. R.; Otero-de-la-Roza, A. *J. Chem. Theory Comput.* **2012**, *8* (12), 5124−5131.
(39) Fafard, J.; Lyubimova, O.; Stoyanov, S. R.; Dedzo, G. K.; Gusarov, S.; Kovalenko, A.; Detellier, C. *J. Phys. Chem. C* **2013**, *117* (36), 18556−18566.
(40) Huang, W.; Dedzo, G. K.; Stoyanov, S. R.; Lyubimova, O.; Gusarov, S.; Singh, S.; Lao, H.; Kovalenko, A.; Detellier, C. *J. Phys. Chem. C* **2014**, *118* (41), 23821−23834.
(41) Lage, M. R.; Stoyanov, S. R.; Carneiro, J. W. de M.; Dabros, T.; Kovalenko, A. *Energy Fuels* **2015**, *29* (5), 2853−2863.
(42) Greathouse, J. A.; Pike, D. Q.; Greenwell, H. C.; Johnston, C. T.; Wilcox, J.; Cygan, R. T.; Geatches, D. I. *Clays Clay Miner.* **2015**, *63*, 185−198.
(43) Pourmohammadbagher, A.; Shaw, J. M. *Energy Fuels* **2016**, *30* (8), 6561−6569.
(44) Fazelabdolabadi, B.; Alizadeh-Mojarad, A. *Appl. Nanosci.* **2017**, *7*, 155−165.
(45) Downs, R. T.; Hall-Wallace, M. *Am. Mineral.* **2003**, *88*, 247−250.
(46) Bish, D. L. *Clays Clay Miner.* **1993**, *41*, 738−744.
(47) Curtis, M. E.; Cardott, B. J.; Sondergeld, C. H.; Rai, C. S. *Int. J. Coal Geol.* **2012**, *103*, 26−31.
(48) Li, J. J.; Yin, J. X.; Zhang, Y. N.; Lu, S. F.; Wang, W.; Li, J.; Chen, F.; Meng, Y. *Int. J. Coal Geol.* **2015**, *152*, 39−49.
(49) Sposito, G. *The Chemistry of Soils*; Oxford University Press: New York, 2008.
(50) Geatches, D. L.; Greenwell, H. C.; Clark, S. J. *J. Phys. Chem. A* **2011**, *115*, 2658−2667.
(51) Newman, S. P.; Greenwell, H. C.; Coveney, P. V.; Jones, W. *J. Mol. Struct.* **2003**, *647* (1−3), 75.
(52) Martínez, L.; Andrade, R.; Birgin, E. G.; Martínez, J. M. *J. Comput. Chem.* **2009**, *30*, 2157−2164.
(53) Cygan, R. T.; Liang, J. J.; Kalinichev, A. G. *J. Phys. Chem. B* **2004**, *108* (4), 1255−1266.
(54) Vanommeslaeghe, K.; Hatcher, E.; Acharya, C.; Kundu, S.; Zhong, S.; Shim, J.; Darian, E.; Guvench, O.; Lopes, P.; Vorobyov, I.; et al. *J. Comput. Chem.* **2010**, *31* (4), 671−690.
(55) Bjelkmar, P.; Larsson, P.; Cuendet, M. A.; Hess, B.; Lindahl, E. *J. Chem. Theory Comput.* **2010**, *6* (2), 459−466.
(56) Pastor, R. W.; MacKerell, A. D., Jr *J. Phys. Chem. Lett.* **2011**, *2* (13), 1526−1532.
(57) Wright, L. B.; Walsh, T. R. *J. Chem. Phys.* **2012**, *137*, 224702.
(58) Skelton, A.; Fenter, P.; Kubicki, J. D.; Wesolowski, D. J.; Cummings, P. T. *J. Phys. Chem. C* **2011**, *115* (5), 2076−2088.
(59) Hess, B.; Kutzner, C.; van der Spoel, D.; Lindahl, E. *J. Chem. Theory Comput.* **2008**, *4* (3), 435−447.
(60) Pronk, S.; Páll, S.; Schulz, R.; Larsson, P.; Bjelkmar, P.; Apostolov, R.; Shirts, M. R.; Smith, J. C.; Kasson, P. M.; van der Spoel, D.; et al. *Bioinformatics* **2013**, *29*, 845−854.
(61) Zhou, Y. S.; Littke, R. *Mar. Pet. Geol.* **1999**, *16*, 771−792.
(62) Humphrey, W.; Dalke, A.; Schulten, K. *J. Mol. Graphics* **1996**, *14*, 33−38.
(63) Maolin, S.; Fuchun, Z.; Guozhong, W.; Haiping, F.; Chunlei, W.; Shimou, C.; Yi, Z.; Jun, H. *J. Chem. Phys.* **2008**, *128* (13), 134504.
(64) Do, D. D.; Do, H. D. *Chem. Eng. Sci.* **2005**, *60*, 1977−1986.
(65) Severson, B. L.; Snurr, R. Q. *J. Chem. Phys.* **2007**, *126*, 134708.
(66) Davidchack, R. L.; Laird, B. B.; Roth, R. *Condens. Matter Phys.* **2016**, *19* (2), 1−10.
(67) Christenson, H. K.; Gruen, D. W. R.; Horn, R. G.; Israelachvili, J. N. *J. Chem. Phys.* **1987**, *87* (3), 1834−1841.
(68) Dirand, M.; Bouroukba, M.; Chevallier, V.; Petitjean, D.; Behar, E.; Ruffier-Meray, V. *J. Chem. Eng. Data* **2002**, *47* (2), 115−143.
(69) Chen, G.; Lu, S.; Zhang, J.; Xue, Q.; Han, T.; Xue, H.; Tian, S.; Li, J.; Xu, C.; Pervukhina, M. *Fuel* **2017**, *199*, 14−21.
(70) Kareem, R. M. A.; Cubillas, P.; Gluyas, J.; Bowen, L.; Hillier, S.; Greenwell, H. C. *J. Pet. Sci. Eng.* **2017**, *149*, 436−455.

DOI: 10.1021/acs.energyfuels.7b02763
Energy Fuels 2018, 32, 1155−1165